Modeling of Adsorption on Nongraphitized Carbon Surface: GCMC Simulation Studies and Comparison with Experimental Data

D. D. Do* and H. D. Do

Department of Chemical Engineering, University of Queensland, St. Lucia, Queensland 4072, Australia

Received: April 18, 2006; In Final Form: June 15, 2006

We model nongraphitized carbon black surfaces and investigate adsorption of argon on these surfaces by using the grand canonical Monte Carlo simulation. In this model, the nongraphitized surface is modeled as a stack of graphene layers with some carbon atoms of the top graphene layer being randomly removed. The percentage of the surface carbon atoms being removed and the effective size of the defect (created by the removal) are the key parameters to characterize the nongraphitized surface. The patterns of adsorption isotherm and isosteric heat are particularly studied, as a function of these surface parameters as well as pressure and temperature. It is shown that the adsorption isotherm shows a steplike behavior on a perfect graphite surface and becomes smoother on nongraphitized surfaces. Regarding the isosteric heat versus loading, we observe for the case of graphitized thermal carbon black the increase of heat in the submonolayer coverage and then a sharp decline in the heat when the second layer is starting to form, beyond which it increases slightly. On the other hand, the isosteric heat versus loading for a highly nongraphitized surface shows a general decline with respect to loading, which is due to the energetic heterogeneity of the surface. It is only when the fluid−fluid interaction is greater than the surface energetic factor that we see a minimum−maximum in the isosteric heat versus loading. These simulation results of isosteric heat agree well with the experimental results of graphitization of Spheron 6 (Polley, M. H.; Schaeffer, W. D.; Smith, W. R. *J. Phys. Chem.* **1953**, *57*, 469; Beebe, R. A.; Young, D. M. *J. Phys. Chem.* **1954**, *58*, 93). Adsorption isotherms and isosteric heat in pores whose walls have defects are also studied from the simulation, and the pattern of isotherm and isosteric heat could be used to identify the fingerprint of the surface.

1. Introduction

Adsorption of gases in porous materials has been studied with density functional theory (DFT) and Monte Carlo (MC) simulations,[3−8] and its study is standard in the characterization of isotherms. Most of the studies on adsorption in the literature are limited to well-defined surfaces, such as crystalline surfaces of graphitized thermal carbon black (GTCB). Unfortunately, real surfaces are far from that ideal situation, and assuming a perfect surface to study adsorption in pores could lead to serious errors in the determination of adsorption isotherms. In this paper, we propose a new model for nongraphitized surface of carbon black, and GTCB is a special case of this model. This model will be described in detail in section 3, and once the configuration of the surface has been constructed, we apply the grand canonical Monte Carlo (GCMC)[3,4] simulation method to study the adsorption behavior of argon. To simulate the extent of graphitization (that is, surfaces obtained from graphitization at different temperatures), there are two surface parameters that characterize the nongraphitization. They are the percentage of carbon atoms that are missing from the top surface layer and the size of the defect resulted from the missing carbon atoms. The simulation results of adsorption isotherm and isosteric heat will be compared with the experimental results of Polley et al.[1] and Beebe and Young.[2] The pattern of increasing isosteric heat with loading in the monolayer coverage of graphitized surface disappears as the surface becomes less graphitized, and when the surface eventually loses its crystalline structure the isosteric heat will decrease with loading even in the monolayer coverage region (the surface energetic heterogeneity has a greater effect than the fluid−fluid interaction). The agreement between the simulation results and the experimental data is a positive step for further application of this general model to study adsorption in porous solids. We will show this with pores of different widths, and in pores beside the surface energetic heterogeneity and the fluid−fluid interaction, the overlapping of the solid−fluid potentials is another factor in controlling the pattern of isotherm and isosteric heat.

2. Potential Energy

2.1. Fluid−Fluid Potential Energy. The interaction energy between two isolated argon atoms can be effectively calculated from the classical 12−6 Lennard-Jones (LJ) potential equation:

$$\varphi_{i,j} = 4\epsilon^{(f,f)}[(\sigma^{(f,f)}/r_{i,j})^{12} - (\sigma^{(f,f)}/r_{i,j})^{6}] \qquad (1)$$

where subscripts are used to denote particles; $r_{i,j}$ is the separation distance between particles i and j. Other equations, such as the Buckingham Exp-6[9] or rather complex equations,[10] could be used, but the LJ 12−6 equation (eq 1) has been proven to perform well for argon, including the vapor−liquid equilibria and the supercritical region provided the pressure is not exceedingly high,[11] and in adsorption on graphitized thermal carbon black.[12−14] For molecular parameters the values of $\sigma =$ 3.405 Å and $\epsilon/k = 119.8$ K have been commonly used in the literature, and they will be used in this work.

2.2. Solid−Fluid Interaction Energy. For the solid−fluid interaction with graphene layers below the top layer with defects

* To whom correspondence should be addressed. Phone: +61-7-3365-4154. Fax: +61-7-3365-2789. E-mail: duongd@cheque.uq.edu.au.

10.1021/jp062386r CCC: $33.50
Published on Web 08/15/2006

("defected" layer), we use the well-known 10−4−3 Steele potential[15]

$$\varphi_{i,s} = 4\pi\rho_s\epsilon^{(f,s)}[\sigma^{(f,s)}]^2\left\{\frac{1}{5}\left(\frac{\sigma^{(f,s)}}{z}\right)^{10} - \frac{1}{2}\left(\frac{\sigma^{(f,s)}}{z}\right)^{4} - \frac{[\sigma^{(f,s)}]^4}{6\Delta(0.61\Delta + z)^3}\right\} \quad (2)$$

where ρ_s is the density of carbon atom per unit surface area of the graphite layer ($\rho_s = 0.382$ Å^{-2}) and Δ is the spacing between two adjacent graphene layers (3.35 Å). The solid−fluid molecular parameters, the collision diameter and the interaction energy, are calculated from the Lorentz−Berthelot mixing rule. The molecular parameters of a carbon atom in the graphite layer are $\sigma^{(s,s)} = 3.4$ Å and $\epsilon^{(s,s)}/k = 28$ K.

To calculate the solid−fluid potential with the top defected layer, we use the summation of pairwise potentials between the particle and all carbon atoms in the defected layer. The pairwise potential is assumed to take the LJ 12−6 equation as in eq 1 with the collision diameter and the well depth of interaction energy being those for solid−fluid interaction.

2.3. Grand Canonical Monte Carlo Simulation. In the grand canonical Monte Carlo (GCMC) simulation, we specify the temperature, volume (pore volume), and chemical potential. To relate the chemical potential and pressure, we use the equation of state for LJ fluid.[16] The parameters associated with the MC simulation used in this paper are (i) the box length is at least 10 times the collision diameter, (ii) the cutoff radius is half the box length, (iii) the number of cycles for the equilibration step is 50 000 and that for the statistics collection is also 50 000, and (iv) in each cycle, there are N displacement moves and N attempts of insertion/removal with equal probability. The simulation box has two surfaces forming the boundaries in the z-direction, and the periodic boundary conditions are applied in the x- and y-directions. For an open surface, we choose the pore width large enough that the adsorption is that on two independent surfaces.

Because we have the defected layer on the top of the surface, we have to define the pore density or surface excess in an unambiguous manner. The surface excess is defined as the ratio of the difference between the number of particles in the simulation box and the number of particles if the *accessible volume* is filled with gases at the bulk density to the surface area as determined by the BET method. The accessible volume and the theoretical BET surface area will be discussed in detail in section 3. Let us for the moment assume that we know these quantities, and the surface excess is given by

$$\Gamma = \frac{\langle N\rangle - V'\rho_b}{S_{BET}} \quad (3)$$

where $\langle N\rangle$ is the ensemble average of the number of particles in the simulation box, V' is the accessible volume, and S_{BET} is the BET surface area determined from the simulation.

The absolute pore density can be defined as the ensemble average of the number of particles per unit accessible volume, and the excess pore density is the difference between the absolute pore density and the bulk gas density:

$$\langle\rho\rangle = \frac{\langle N\rangle}{V'}; \qquad \langle\rho\rangle_{excess} = \frac{\langle N\rangle}{V'} - \rho_b \quad (4)$$

2.4. Isosteric Heat. A thermodynamic quantity of interest in adsorption studies is the isosteric heat, which is the heat released for each molecule added to the adsorbed phase. Using the fluctuation theory, the isosteric heat is calculated from[4]

$$q_{iso} = \frac{\langle U\rangle\langle N\rangle - \langle UN\rangle}{\langle N^2\rangle - \langle N\rangle\langle N\rangle} + kT = \left[\frac{\langle U_{ff}\rangle\langle N\rangle - \langle U_{ff}N\rangle}{\langle N^2\rangle - \langle N\rangle\langle N\rangle} + kT\right] + \frac{\langle U_{sf}\rangle\langle N\rangle - \langle U_{sf}N\rangle}{\langle N^2\rangle - \langle N\rangle\langle N\rangle} \quad (5)$$

where $\langle\ \rangle$ is the ensemble average; N is the number of particles and U is the configuration energy of the system. The second equality of eq 5 shows two contributions to the isosteric heat: one is due to the fluid−fluid interaction and the other is due to the fluid−solid interaction, that is, $U = U_{ff} + U_{sf}$.

3. Model of a Nongraphitized Carbon Surface

There are different approaches in the literature that model an amorphous surface. For example, Bakaev[17] considered a rumpled graphite basal plane to model a heterogeneous surface. The atomic structure of this surface is obtained by squeezing the graphite surface in a molecular dynamics simulation with a random initial velocity of each atom on the graphite surface. Another model for amorphous surface has been proposed.[18] In this model a surface containing 50% sp^3-bonded atoms and a density of about 3 g/cm^3 was constructed using molecular dynamics DFT to yield a cluster of 64 carbon atoms, and then the final solid was the replication of the original cluster. A similar version was adopted by these authors using a Bernal formulation, in which a box containing 1000 carbon atoms with a diameter of 3.08 Å, which is twice the C−C bond length in diamond, is simulated to produce a carbonaceous solid having an apparent density close to that of the real solid. Another approach for dealing with an amorphous surface is through the functional form of solid−fluid potential rather than the physical model of the surface. This approach was adopted by Kuchta and Firlej,[19,20] who superimposed the Steele 10−4−3 equation with a function in x- and y-distances to describe the degree of modulation of the surface.

3.1. New Model for Nongraphitized Surface. In this paper we shall model a nongraphitized surface as a collection of graphene layers with the top layer being a defected one. In general, we could introduce defects in all layers, but for simplicity we will consider all layers to be perfect graphene layers, except the top one. To model defects of the top layer, we select at random a carbon atom in the top layer and remove it as well as all surrounding neighbors that have distances to the selected atom less than an effective defect radius R_c. We repeat this random selection until the percentage of carbon atoms removed has reached a given defect percentage. Thus the two important parameters for modeling a nongraphitized surface are the percentage of defect and the size of the defect, which is measured by the effective radius, R_c. Figure 1 shows the top layers of carbon surfaces with various degrees of defect from 0 to 30%. As the degree of defect increases, it is seen that the surface loses its crystallite structure, and it becomes amorphous when the percentage of defect is greater than 30%.

3.2. Determination of Accessible Volume and BET Surface Area. Having defined the surface with defects by random removal of carbon atoms, it is necessary to develop a Monte Carlo approach to calculate the accessible pore volume as this is required to calculate the average pore density and the surface excess. We choose a simulation box shown as dashed lines in Figure 2. Because the top layers of the two walls have defects and the percentage of defects could be close to 100%, it is

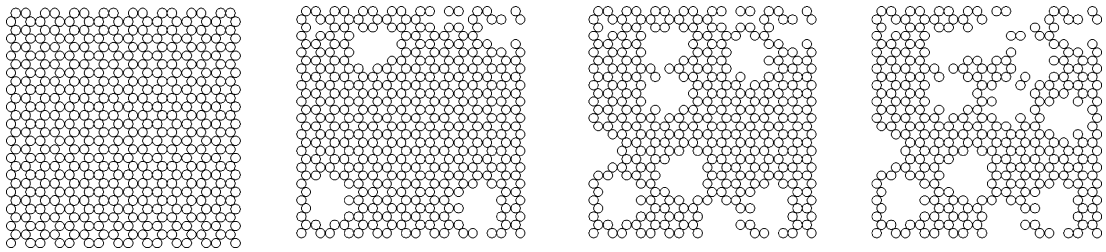

Figure 1. Configuration of the top surface of nongraphitized carbon black. From left to right, the percentage of defect is 0, 10, 20, and 30%, and the effective defect radius is 2.84 Å.

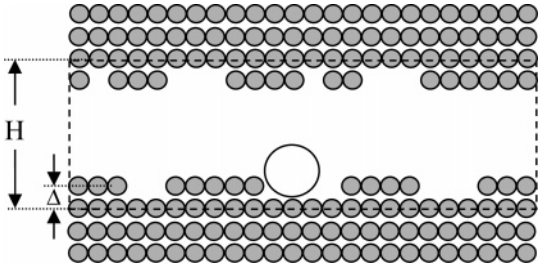

Figure 2. Simulation box to determine the accessible volume.

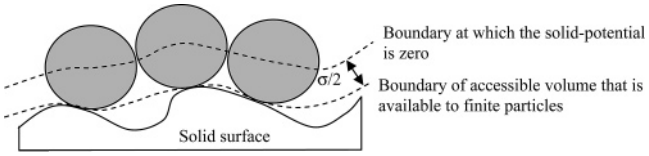

Figure 3. Schematic diagram of the accessible volume for particle centers (boundary is the loci of zero solid−fluid potential energy, the top dashed line) and the accessible volume for particles whose boundary is the bottom dashed line.

convenient to define the physical pore width as the distance between the plane passing through all carbon centers of the layer just underneath the top defected layer and the corresponding plane of the opposite wall (see Figure 2 for this definition).

A particle is randomly inserted into the simulation box, and the solid−fluid potential energy is calculated between this particle and all the carbon atoms. If the potential energy is negative or zero, we count this particle and then remove it from the box. This process is repeated so that some meaningful statistical average can be obtained. In this work, we use 10 million attempts of insertion, and the percentage of accepted particles is calculated and is taken to be the ratio of the accessible volume to the simulation box volume. This accessible volume is actually the volume that is available only to the *center* of a particle, not the whole particle. Because a particle has a finite volume that is characterized by the collision diameter, we need to determine the accessible volume that is available to the whole particle. To do this, we adopt a simple geometric consideration in that if we know the "surface area" we can determine the accessible volume for the whole particle as the sum of the accessible volume available to the centers and the extra volume accounting for the finite size of the adsorbate. This extra volume is $S\sigma/2$, where S is the surface area of one surface and σ is the collision diameter (Figure 3).

The question then is, how do we estimate the surface area of an amorphous surface? The surface is microscopically fractal because it is composed of discrete atoms; its area depends on the yardstick that one uses for this purpose. The yardstick in our context of adsorption is the collision diameter of the probe molecule. We will adopt the BET surface area, which is derived from the theoretical isotherm that is simulated from the grand canonical Monte Carlo simulation of adsorption of a probe on the amorphous surface. Thus, to determine the surface area, we

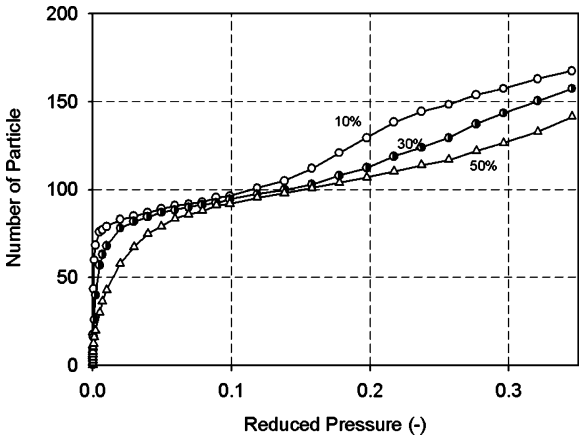

Figure 4. GCMC-simulated adsorption isotherm of nitrogen on various surfaces of linear dimension of 36.15 Å, with defects. The effective defect radius is 2.84 Å.

TABLE 1: GCMC Surface Area of Surfaces with Various Degrees of Defect[a]

degree of defect, %	no. of nitrogen particles to form a monolayer	monolayer area, Å^2	increase in area, %
10	94	1520	1500
40	90	1463	12
50	91	1473	13

[a] The effective defect radius is 2.84 Å.

carry out the simulation to obtain a "numerically experimental" isotherm and this mimics exactly what one would do experimentally. Let us assume that nitrogen is the standard molecular probe used in the surface area determination. We carry out the simulation of nitrogen adsorption on a defected surface, and obtain the number adsorbed as a function of pressure in the reduced pressure range from 0.05 to 0.30. Next, we apply the linearized BET plot to determine the surface area with the projection area of nitrogen of 16.2 Å^2.[21] Once the area of the defected surface has been determined, we determine the accessible pore volume to the whole particle.

3.3. Illustration of BET Surface Area. As an illustration of the determination of BET surface area, we perform a GCMC simulation of nitrogen adsorption on surfaces with various percentages of defect and the effective defect radius of 2.84 Å. The box length of the simulation box is 36.15 Å (10 times the collision diameter of nitrogen, $\sigma_{\text{Nitrogen}} = 3.615$ Å). The well depth of interaction energy of nitrogen is 101.5 K.[22] The equilibrium number of particles is plotted against reduced pressure ranging from 0.01 to 0.35 as shown in Figure 4, and the linearized BET plot is carried out. Good linearity is achieved for the reduced pressure from 0.01 to 0.2. For example, in the case of 30% defect, the number of particles required to form a monolayer is $N_m = 93$. Taking the projection area of nitrogen as 16.2 Å^2, the surface area is calculated as 1500 Å^2. If the surface is perfectly flat (i.e., without defect), the geometric

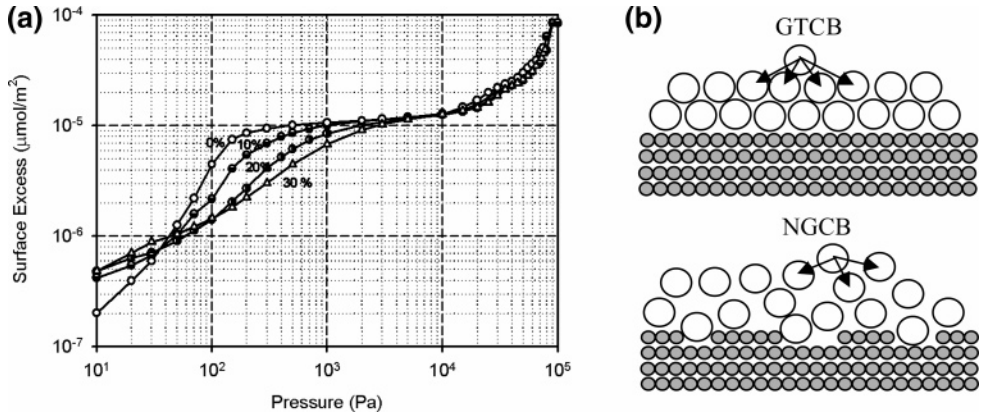

Figure 5. (a) Adsorption of argon at 87.3 K on nongraphitized carbon black with effective radius of 2 times the carbon−carbon bond length (R_c = 2.84 Å). The percentage of defect varies from 0 to 30%. (b) Schematic diagram of molecular interaction at higher layers for NGCB and GTCB.

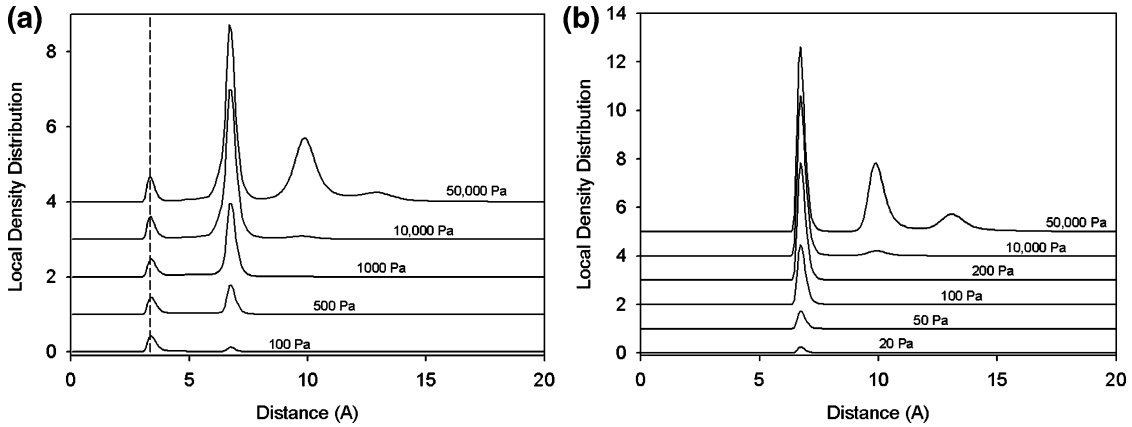

Figure 6. (a) Local density distribution of argon adsorption on NGCB with 30% defect and the effective defect radius of 2.84 Å. Adsorption temperature is 87.3 K. (b) Local density distribution on GTCB at the same temperature.

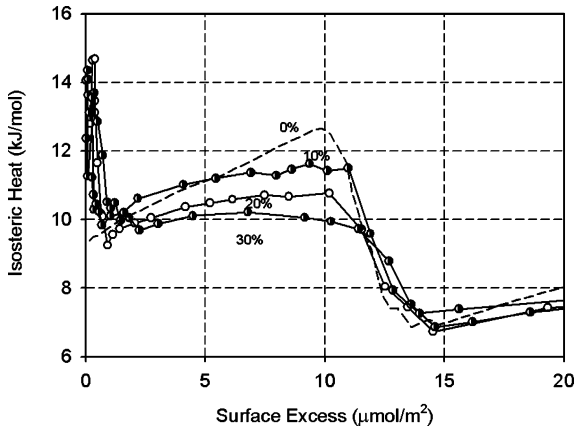

Figure 7. Isosteric heat of adsorption of argon on nongraphitized carbon black with effective radius of 2 times the carbon−carbon bond length (R_c = 2.84 Å). The percentage of defect varies from 0 to 30%, and the adsorption temperature is 87.3 K.

surface area is $(36.15\ \text{Å})^2 = 1307\ \text{Å}^2$. The area of 30% defected surface is 15% greater than that of the flat geometric surface. Table 1 shows the number of nitrogen particles to form a monolayer coverage, the corresponding area, and the percentage increase relative to the flat surface for surfaces of various percentages of defect.

4. Results and Discussion

We have presented the necessary ingredients for the simulation of adsorption on a nongraphitized carbon black. We now investigate how the various parameters would affect the behaviors of adsorption isotherm and isosteric heat.

4.1. Adsorption on Nongraphitized Carbon Black Surface. Good description of adsorption of argon on GTCB has been presented in some of our earlier publications,[12−14] including isosteric heat. In this paper we concentrate on adsorption behaviors on nongraphitized carbon black (NGCB) and compare them with GTCB.

Effects of the Extent of Defect. Figure 5a shows the adsorption isotherm of argon on NGCB at 87.3 K with various degrees of defect, measured as the percentage of carbon atoms that are missing from the top layer. In this figure, the effective defect radius is chosen as 2 times the carbon−carbon bond length (R_c = 2.84 Å). We see that the adsorption isotherm has a wavelike behavior when the surface is perfect (no defect) and takes a smoother behavior when the extent of defect is increased. The waviness of the perfect graphite surface is because the first adsorbed layer is perfectly parallel to the surface and before the monolayer is completed any addition of molecules into the system will result in its adsorption into the first adsorbed layer as this will give not only good fluid−fluid interaction but also good solid−fluid interaction, yielding the lowest potential energy. This effect fades at higher layers as the solid−fluid interaction becomes weaker, lending to a greater contribution of the fluid−fluid interaction. On the other hand, when the surface has a fair amount of defects, the isotherm is smoother and there is no clear plateau of monolayer coverage for the case of NGCB. This is simply due to the irregular packing in the case of NGCB, compared to a much more ordered layering in the case of graphitized thermal carbon black (Figure 5b).

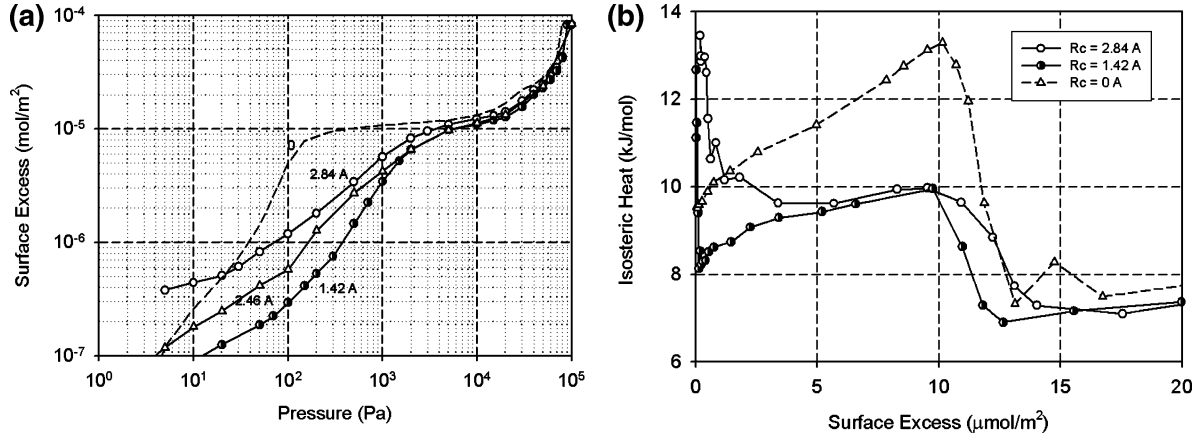

Figure 8. (a) Adsorption of argon on nongraphitized carbon black at 87.3 K with the percentage of defect being 30%. The effective radius is 0, 1.42, 2.46, and 2.84 Å. (b) Isosteric heat of adsorption of argon.

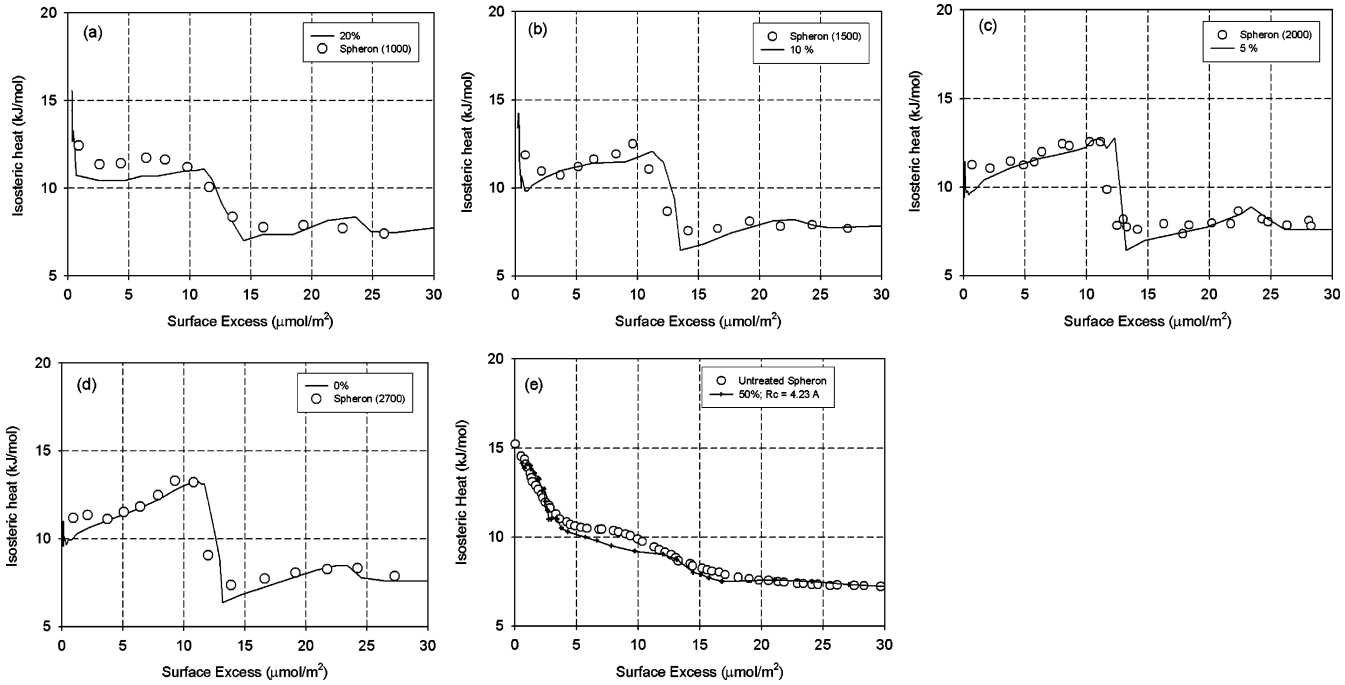

Figure 9. Comparison between experimental isosteric heat data and GCMC simulation of adsorption of argon on surfaces of NGCB. (a) Spheron (1000); (b) Spheron (1500); (c) Spheron (2000); (d) Spheron (2700); (e) untreated Spheron.

Interesting, but not surprising, is the behavior of the adsorption isotherm at very low loadings. For GTCB, we see that Henry's law is satisfied (as seen by the slope of unity in the log−log plot). However, in the case of NGCB, Henry's law is never observed because molecules adsorb onto the strongest sites and further adsorption will occur on progressively weaker sites. It is because of this progressive decrease in the adsorption affinity that Henry's law is never observed for NGCB.

To substantiate the adsorption isotherm and the mechanism of molecular interaction as shown in Figure 5, we show the density distributions above the surface at various values of pressure. This is shown in Figure 6a for NGCB and Figure 6b for GTCB for comparison. The local distribution in the case of GTCB shows distinctly narrow peaks, suggesting that adsorbed layers are parallel and reside at fixed distances from the surface. On the other hand, the local distribution in the case of NGCB shows an extra small peak, which is the contribution of molecules residing in the defects in the top layer. This distribution is quite broad, indicating that layers are less distinct, especially in the layer that is close to positions of molecules that reside inthe defects. This supports the schematic adsorption picture of Figure 5b.

From the distributions for NGCB, we see that at low pressures argon particles are localized in the defects as these are strong energy sites. Thus the initial adsorption is localized, which is in contrast to the case of GTCB where the adsorption is completely mobile. When all defects of NGCB are occupied with particles, further adsorption will occur on graphene patches. This adsorption is principally mobile, but it is affected by the localized particles that reside in the defects. As the pressure is further increased, more layers will be formed, but they are not as distinct as those in the case of GTCB. This explains the broader and somewhat overlapping peaks as observed in the distribution.

Having seen the effect of nongraphitization on the isotherms, we now turn our attention to the behavior of isosteric heat versus loading. This is shown in Figure 7 for the case of effective defect radius of 2.84 Å. The simulated isosteric heat for graphitized thermal carbon black is shown as a dashed line for comparison with those of NGCB.

The behavior of GTCB is well-known and will not be discussed here. In the case of NGCB of 30% defect, we see that the isosteric heat at zero loadings is very high (about 15

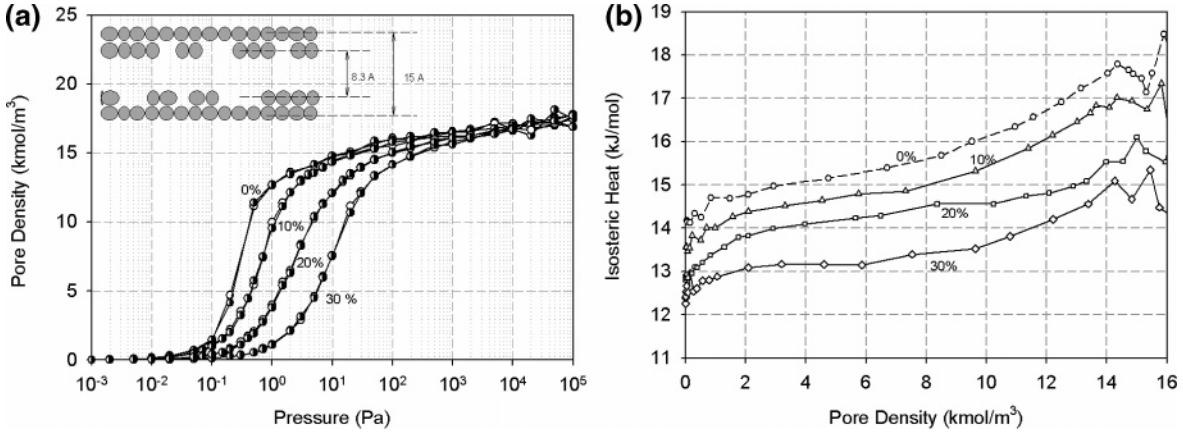

Figure 10. (a) Adsorption isotherm of argon in 8.3 Å slit pores with 0, 10, 20 and 30% defect on the top layers of each wall (the effective defect radius is 2.84 Å). (b) Isosteric heat versus loading for pores of different defects.

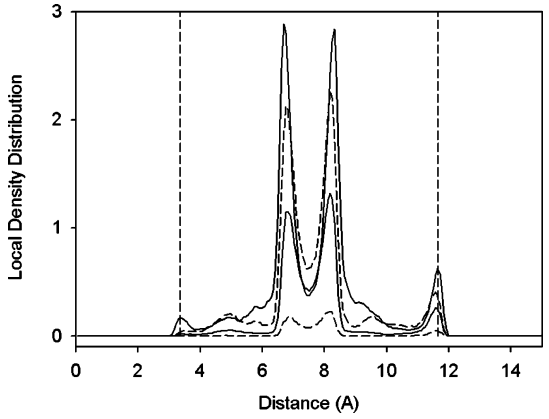

Figure 11. Local density distribution in 8.3 Å pore with 30% defect for pressures of 1, 10, 100, and 100 000 Pa (the lowest curve is for 1 Pa and the highest curve is for 100 000 Pa). The effective defect radius is 2.84 Å.

kJ/mol, compared to 9.5 kJ/mol in the case of GTCB) and this is due to the "local" adsorption into defects that possess the greatest affinity. As the adsorption progresses, molecules will be "locally" adsorbed into defects of progressively lower affinity, and this results in the decrease in the isosteric heat versus loading. When the loading is increased, the isosteric heat is practically constant and this constancy is a balance between the surface energetic heterogeneity and the fluid−fluid interaction caused by mobile molecules outside the defected areas. Finally, when loading is increased further (loading is greater than about 10 μmol/m^2), the isosteric heat will decrease and this is because molecules are now further from the surface, giving lower solid−fluid interaction. The results obtained thus far show a sharp difference in the characteristics of adsorption on a heterogeneous surface and that on a perfectly homogeneous surface. The difference is clearly manifested in the heat curve versus loading and the lack of Henry law behavior in the adsorption isotherm. Combining the behavior of isosteric heat versus loading and the pattern of isotherm could be used as a fingerprint of the defected surface.

Effects of the Effective Defect Radius. To see the effects of the radius of the defect, we show in Figure 8a the adsorption isotherms of argon at 87.3 K on a surface with 30% defect and the effective radius of defect takes the following values: 1.42, 1.42 $\sqrt{3}$, and 2.84 Å. If the defect radius is 1.42 Å, the hole is too small to create any high-energy site and therefore its adsorption isotherm is below that for the case of GTCB because each argon particle has a lesser number of carbon atoms to interact with. It is only when the effective defect radius is 2.84 Å (twice the carbon−carbon bond length) that we see the presence of high-energy sites, which are basically the holes of the top layer that is large enough to trap argon particles.

What we have observed in the isotherm plots is supported by the plot of isosteric heat versus loading as shown in Figure 8b.

Comparison with Experimental Data. Experimental data for adsorption on surfaces with various degrees of graphitization are scarce in the literature. As far as the authors are aware of, the only data are those of argon adsorption on surfaces with different degrees of graphitization from the work of Polley et al.[1] and Beebe and Young.[2] The nonporous carbon black used by Beebe and Young is Spheron 6 (rubber reinforcing channel black), whose surface area is 115 m^2/g and particle size is 280 Å.[23] This sample was subjected to heat treatment for 2 h at various temperatures to produce four samples: Spheron (1000), Spheron (1500), Spheron (2000), and Spheron (2700). The numbers in parentheses are the treatment temperatures.

Figure 9 shows the experimental isosteric heat data of argon (circles) on surfaces of varying degrees of graphitization at 77 K.[2] The heat curve for Spheron (1000) indicates the dominance of the surface heterogeneity over the fluid−fluid interaction, while that of Spheron (2700) indicates the opposite. Using the GCMC simulation results for argon adsorption at 77 K on surfaces of various degrees of defect, we have found that the simulation results for the surfaces with 20, 10, 5, and 0% defect and the effective defect radius of 2.84 Å yield heat curves that are in good agreement with Spheron samples treated thermally at 1000, 1500, 2000 and 2700 °C, respectively. This means that Spheron (2700) behaves very much like a homogeneous graphite surface, which is known in the literature. Regarding the other samples, for example Spheron (1500) has 10% defect on the surface. The agreement of the isosteric heat versus loading for argon adsorption on surfaces of different degrees of graphitization suggests that the model proposed in this paper has potential for wider applications.

Beside the heat curves for the four heat-treated samples, Beebe and Young[2] also presented the heat curve for the untreated Spheron sample. The isosteric heat curve versus loading for this untreated sample indicates that it is a very heterogeneous surface (circles in Figure 9e) because the isosteric heat decreases continuously versus loading. Because it is very heterogeneous, we simulate the surface with a very high extent of defect (50%) and a larger effective defect radius of 4.23 Å (compared to 2.84 Å in the cases of heat-treated samples) and find that the isosteric heat curve has a pattern similar to that

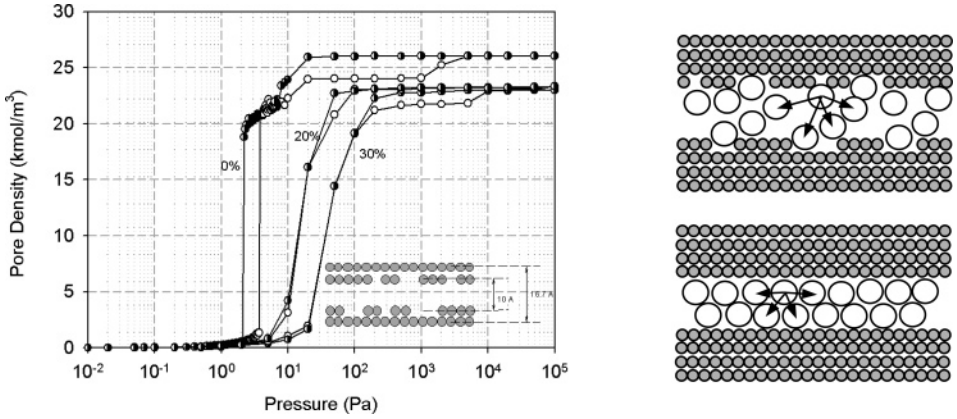

Figure 12. Adsorption isotherm of argon in 10 Å pores of different degrees of defect (0−30%). The effective defect radius is 2.84 Å.

observed experimentally. The agreement between our simulation results and the data is very good.

4.2. Adsorption in Pores with Surface Defects. We have seen the significance of the nongraphitization of the adsorption isotherms and isosteric heat versus loading for open surfaces. Let us now turn to the investigation of this nongraphitization on the adsorption in pores whose walls have defects on the top layer. In this investigation we will see the interplay not only between the surface heterogeneity and the fluid−fluid interaction but also with the overlapping of potentials exerted by two walls of the pore. We shall choose a couple of representative pores to illustrate our point. These pores are 8.3 and 10 Å. The first pore is slightly too large for one layer and too small for two layers, and the second pore (10 Å) can accommodate two layers. The count of the number of layers excludes those molecules that reside inside the defects of the top layers.

Slit Pore 8.3 Å: Effects of the Percentage of Defect. Figure 10a shows the adsorption isotherm at 87.3 K in an 8.3 Å pore with the top layers of each wall having various percentages of defect. The pore that has greater defects has slower uptake of adsorbates. Although pores with defects have slower uptake, the maximum capacity is the same as that for a perfect pore; i.e., the defect is not great enough to disturb the packing. For this pore width, the adsorption isotherm is reversible, irrespective of the extent of the defect.

The corresponding isosteric heats are shown in Figure 10b. The isosteric heat of all defected pores is lower than that of the perfect pore (0% defect) at all loadings. This seems to be a surprise at first, but the lower heat of the defected surfaces for this very small pore is due to the dominance of the overlapping of potentials exerted by the two opposite walls over the surface heterogeneity. This is supported by the density distribution in Figure 11.

At low pressures, peaks are mainly observed in the pore interior. This is due to the dominance of the overlapping of potentials exerted by the two walls of the pore. The middle two peaks overlap somewhat, and this is the indication that the pore is a bit too large for one layer and too small for two layers. Another observation that can be derived from this distribution is that the middle two peaks are not symmetrical at low loadings, and this is because the defects are created randomly and the bottom defected layer is not the same as the top defected layer even though they have the same percentage of defect. At high loadings, molecules enter the pore and fill the pore interior as well as the defect sites.

Pore 10 Å with Defects. Next we show the adsorption isotherms in 10 Å pores as shown in Figure 12. This pore can accommodate exactly two layers of molecules in the perfect pore (no defects). The adsorption isotherm of this perfect pore shows a sharp transition in density from a gaslike state to a liquidlike state at a pressure of about 4 Pa, and this is due to the favorable combined solid−fluid and fluid−fluid interactions. On desorption, evaporation occurs at a lower pressure of about 2 Pa, resulting in hysteresis in this perfect pore. Upon formation of a liquidlike phase in the pore ($P > 4$ Pa), there is another hysteresis and this is associated with the compression of the adsorbed phase.

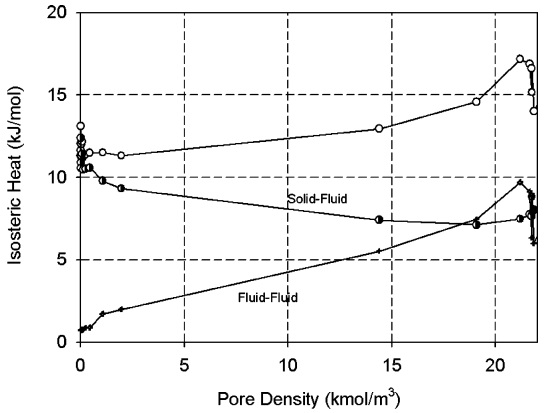

Figure 13. Isosteric heat as a function of loading for adsorption of argon in 10 Å pore at 87.3 K. The percentage of defect is 30%, and the effective defect radius is 2.84 Å.

Let us now turn our attention to the effects of the defect. In the same figure we show isotherms of pores with different extents of defect (20 and 30%) and the effective defect radius of 2.84 Å. We see that the defect destroys the 0−1 transition (which is observed with the perfect pore), and this is simply due to the lower fluid−fluid interaction energy because of the longer average distance between neighboring atoms compared to that of the perfect pore (see the inset of Figure 12). This is also supported by the fact that the maximum pore density (density at saturation pressure) is greater in the perfect pore. The reason the defected pore cannot achieve high packing is that there are "local" sites (where the defects are) whose affinities are high enough for molecules on those sites to be moved around in order to maximize the packing.

The isosteric heat versus loading for the case of defected pore with 30% defect and $R_c = 2.84$ Å is shown in Figure 13. To explain for the observed behavior, we have to consider the separate contributions of solid−fluid and fluid−fluid interactions. The solid−fluid contribution shows a steady decrease with loading, indicating that adsorption occurs at the high-energy sites first and further adsorption occurs on progressively weaker sites. The fluid−fluid contribution, as

expected, shows a steady increase with loading due to the increase of neighboring atoms, and as the loading is very high, we observe a drop in the heat contributed by the fluid−fluid interaction. This is due to the repulsion between highly dense adsorbed particles.

5. Conclusions

We have presented in this paper a new model to describe a surface of nongraphitized carbon black. The surface is composed of multiple layers of graphene with the top one having defects. The defective top layer is created by randomly removing carbon atoms from it. The two parameters that characterize the defective top surface are the percentage of carbon removal and the effective defect size. This model is used in the GCMC simulations of argon adsorption, and very rich patterns of isotherms as well as isosteric heat versus loading are obtained. The simulation results are in good agreement with the experimental data of isosteric heat for Spheron 6 subject to different heat treatments.[2] The rich pattern is the result of the interplay of the surface energetic heterogeneity, the lateral fluid−fluid interaction, and the overlapping of potentials exerted by the two walls. We illustrate this with adsorption of argon on open surfaces as well as in pores of various sizes, and this model has been proven to be a potential one for future studies of adsorption in activated carbon.

Acknowledgment. Support from the Australian Research Council is gratefully acknowledged.

References and Notes

(1) Polley, M. H.; Schaeffer, W. D.; Smith, W. R. *J. Phys. Chem.* **1953**, *57*, 469.
(2) Beebe, R. A.; Young, D. M. *J. Phys. Chem.* **1954**, *58*, 93.
(3) Allen, M. P.; Tildesley, D. J. *Computer Simulation of Liquids*; Clarendon Press: Oxford, 1987. Frenkel, D.; Smit, B. *Understanding Molecular Simulations*; Academic Press: New York, 2002.
(4) Nicholson, D.; Parsonage, N. *Computer Simulation and the Statistical Mechanics of Adsorption*; Academic Press: London, 1982.
(5) El-Merraoui, M.; Aoshima, M.; Kaneko, K. *Langmuir* **2000**, *16*, 4300.
(6) Tanaka, H.; El-Merraoui, M.; Kodaira, T.; Kaneko, K. *Chem. Phys. Lett.* **2002**, *351*, 417.
(7) Ravikovitch, P.; Vishnyakov, A.; Neimark, A. *Phys. Rev. E* **2001**, *64*, 011602. Vishnyakov, A.; Ravikovitch, P.; Neimark, A. *Langmuir* **1999**, *15*, 8736. Neimark, A.; Ravikovitch, P. *Langmuir* **1997**, *13*, 5148.
(8) Steele, W. A. *Appl. Surf. Sci.* **2002**, *196*, 3.
(9) Mason, E. A.; Rice, W. *J. Chem. Phys.* **1954**, *22*, 843.
(10) Barker, J.; Fischer, R.; Watts, R. *Mol. Phys.* **1971**, *21*, 657.
(11) Hauschild, T.; Prausnitz, J. *Mol. Simul.* **1993**, *11*, 177.
(12) Do, D. D.; Do, H. D. *Langmuir* **2004**, *20*, 7103.
(13) Do, D. D.; Do, H. D. *Fluid Phase Equilib.* **2005**, *236*, 169.
(14) Do, D. D.; Do, H. D. *J. Colloid Interface Sci.* **2005**, *287*, 452.
(15) Steele, W. A. *Surf. Sci.* **1973**, *36*, 317.
(16) Johnson, J. K.; Zollweg, J.; Gubbins, K. E. *Mol. Phys.* **1993**, *78*, 591.
(17) Bakaev, V. A., *J. Chem. Phys.* **1995**, *102*, 1398. Bakaev, V.; Steele, W. A. *Adsorpt. Sci. Technol.* **1993**, *10*, 123.
(18) Cascarini de Torre, L. E.; Bottani, E. J. *Langmuir* **1995**, *11*, 221.
(19) Kuchta, B.; Firlej, L. *Stud. Surf. Sci. Catal.* **2005**, *156*, 683.
(20) Kuchta, B.; Llewellyn, P.; Denoyel, R.; Firlej, L. *Colloids Surf., A* **2004**, *241*, 137.
(21) Kruk, M.; Li, Z.; Jaroniec, M.; Betz, W. *Langmuir* **1999**, *15*, 1435.
(22) Ravikovitch, P.; Vishnyakov, A.; Russo, R.; Neimark, A. *Langmuir* **2000**, *16*, 2311.
(23) Schaeffer, W. D.; Smith, W. R.; Polley, M. H. *Ind. Eng. Chem.* **1953**, *45*, 1721.